

DINO-LG: A Task-Specific DINO Model For Coronary Calcium Scoring

Mahmut Selman Gokmen^{a,*}, Caner Ozcan^{a,b}, Moneera N. Haque^a,
Steve W. Leung^a, C. Seth Parker^a, W. Brent Seales^a and
Cody Bumgardner^a

^aUniversity of Kentucky Lexington USA

^bDepartment of Software Engineering Karabuk University Turkey

ARTICLE INFO

Keywords:

Deep Learning

Foundational Models

Coronary Artery Calcification

Segmentation

DINO

ABSTRACT

Coronary artery disease (CAD), one of the leading causes of mortality worldwide, necessitates effective risk assessment strategies, with coronary artery calcium (CAC) scoring via computed tomography (CT) being a key method for prevention. Traditional methods, primarily based on UNET architectures implemented on pre-built models, face challenges like the scarcity of annotated CT scans containing CAC and imbalanced datasets, leading to reduced performance in segmentation and scoring tasks. In this study, we address these limitations by incorporating the self-supervised learning (SSL) technique of DINO (self-distillation with no labels), which trains without requiring CAC-specific annotations, enhancing its robustness in generating distinct features. The DINO-LG model, which leverages label guidance to focus on calcified areas, achieves significant improvements, with a sensitivity of 89% and specificity of 90% for detecting CAC-containing CT slices, compared to the standard DINO model's sensitivity of 79% and specificity of 77%. Additionally, false-negative and false-positive rates are reduced by 49% and 59%, respectively, instilling greater confidence in clinicians when ruling out calcification in low-risk patients and minimizing unnecessary imaging reviews by radiologists. Further, CAC scoring and segmentation tasks are conducted using a basic UNET architecture, applied specifically to CT slices identified by the DINO-LG model as containing calcified areas. This targeted approach enhances CAC scoring accuracy by feeding the UNET model with relevant slices, significantly improving diagnostic precision, reducing both false positives and false negatives, and ultimately lowering overall healthcare costs by minimizing unnecessary tests and treatments, presenting a valuable advancement in CAD risk assessment.

1. Introduction

Cardiovascular disease (CVD) is the leading cause of death globally, responsible for approximately 17.9 million fatalities in 2019, which constitutes 32% of all deaths worldwide [1]. Coronary artery disease (CAD), a major cardiovascular disease affecting the blood vessels that feed the heart muscle, caused 371,506 deaths in the United States in 2022 [2]. According to the most recent heart disease and stroke statistics report, approximately 5% of adults over the age of 20 have CAD in the United States [3]. Early detection of CAD allows for timely interventions that can prevent progression of the disease and reduce the risk of life-threatening heart attacks. It can also lead to a wider range of treatment options, including lifestyle changes, medications or surgical procedures. The earlier CAD is detected, the more effective these treatments can be. Furthermore, overall treatment costs can be reduced by preventing more serious complications requiring intensive care or extensive procedures.

Coronary artery calcium (CAC) scoring is considered a reliable tool for assessing cardiovascular disease and is generally recommended for use by various medical guidelines [4]. CAC scoring helps identify the presence and extent of calcified plaque in the coronary arteries which is strongly associated with the risk of CAD and future cardiovascular events. The test is non-invasive and relatively simple, using computer tomography (CT) scans to measure calcium deposits without the need for invasive procedures. The risk categorized calcium scores reflect different risk categories for cardiovascular events [5]. Higher CAC scores can lead to more aggressive management of risk factor, while lower scores might support a more conservative approach. It is crucial for the radiographer to evaluate the position of high-density voxels in order to detect coronary calcification. CAC is typically measured using the Agatston method, assessing calcium deposits in the coronary arteries by measuring calcium density and volume to calculate a total calcium score [6].

The Agatston scoring system is a well-established method for quantifying CAC and stratifying cardiovascular risk [7]. Evidence from large cohort studies, such as the Multi-Ethnic Study of Atherosclerosis (MESA), demonstrates a strong association between CAC scores and the risk of adverse cardiovascular events. For instance, in MESA, individuals with a CAC score of 0 were found to have a 10-year cardiovascular event risk of approximately 1%, while those with scores >300 had risks exceeding 20% over the same period. These findings underpin the use of CAC scoring in clinical guidelines, including those from the American College of Cardiology (ACC) and the American Heart Association (AHA), which recommend CAC assessment in intermediate-risk patients (10–20% 10-year ASCVD risk) to refine risk stratification

*This work is the results of the research project supported by the NIH National Center for Advancing Translational Sciences and the Scientific and Technological Research Council of Türkiye (TUBITAK).

*Corresponding author

✉ m.gokmen@uky.edu (M.S. Gokmen)

ORCID(s): 0009-0000-0891-7567 (M.S. Gokmen)

and guide therapeutic decisions. Notably, patients with scores ≥ 100 are often prioritized for statin therapy and other aggressive interventions, while those with a score of 0 may safely defer pharmacological treatments in favor of lifestyle modifications. Currently, the clinical analysis of calcium scores is performed semi-automatically by a software tool used by the radiologist to identify calcium regions by individually checking the slide images of each patient. This CAC measurement can be attention-demanding, labor-intensive, and time-consuming. To address these issues, automated CAC scoring methods have been developed, which can help enhance accuracy, consistency, and efficiency in measurements [8, 9, 10].

Clinically, contrast-enhanced coronary CT angiography is a powerful imaging technique that uses contrast agent to provide detailed images of the coronary arteries to detect obstructive lesions and other vascular abnormalities, but involves higher radiation exposure due to the need for additional imaging sequences and the use of contrast [11]. On the other hand, non-contrast ECG-gated CT scans focus on quantifying coronary artery calcium, synchronizing image acquisition with the cardiac cycle to minimize motion artifacts and accurately assess calcified plaque for cardiovascular risk evaluation. Traditionally, when the CAC score has been calculated using non-contrast ECG-gated CT scans, a significant association with clinical outcomes has been observed [12, 13]. However, other studies have shown that CAC calculation using non-contrast ECG non-gated CT data has excellent agreement with gated data [14, 15, 16, 17]. In this study, we propose a self-supervised learning based CAC scoring method that uses both gated and non-gated CT images together.

Most efforts in deep learning for image analysis have used some form of supervised learning. However, existing supervised learning methods face challenges when there is a lack of labeled data. In public datasets of CT scans, for instance, less than 10% of the total slices contain calcified areas, despite the overall abundance of scans. This scarcity of labeled, relevant data poses a significant challenge for supervised approaches. Additionally, considering that calcifications typically cover only 3-5 millimeters, it becomes evident how challenging this task is. This small size makes accurate detection even more difficult, underscoring the need for advanced methods capable of identifying such minute details in CT scans.

Another learning paradigm that effectively addresses the mentioned data scarcity challenges is self-supervised learning (SSL) [18, 19, 20]. In traditional computer vision tasks, there is typically a large amount of unlabeled data available for SSL methods. SSL holds significant promise for enhancing coronary artery calcium scoring, particularly in the context of limited labeled data. In traditional supervised learning approaches, obtaining sufficient labeled datasets can be challenging and time-consuming, especially in the clinical domain where calcified medical images are often rare. SSL allows models to learn from vast amounts of unlabeled data by extracting features and patterns without the need for explicit annotations [20]. This capability is particularly valuable for CAC scoring, as it enables more robust training

of algorithms to identify calcium deposits in coronary arteries. Furthermore, while several studies have successfully developed automated CAC scoring using supervised learning methods, there is currently no reported method using self-supervised learning model on both gated and non-gated non-contrast ECG CTs.

In this study, we have implemented one of the most popular SSL training technique using vision transformers (ViT) [21] and commonly known as DINO (self-distillation with no labels) [22]. Regarding the architectural design of ViT models, generated features by ViT model in DINO model make possible to use these features in different tasks such as classification, segmentation or detection. In our approach, ViT models trained with DINO technique are utilized to classify CT slices whether containing calcified area. When it is considered that the area covered by calcification in CT slices and the ratio of CT slices containing calcification areas to across all CT slices in dataset, generating the features highlighting and capturing calcification areas is a challenging task.

To overcome this issue and generate the features capturing targeted areas' specifications, we introduce a novel training method, DINO-LG, aimed at enhancing SSL approaches by incorporating label guidance to capture more specific features such as calcified areas in the model's training process. This new technique is designed to contribute to SSL methodologies and expand upon existing training frameworks. Additionally, it has been demonstrated that vision foundational models can be directed toward specific areas, enabling them to generate features that effectively capture desired characteristics.

The contributions of this paper can be summarized as follows:

- We propose a two-stage calcification identification method that first classifies CT slices based on the presence of calcification and then segments the calcifications from the identified slices.
- The success of this method is driven by DINO-LG, a transformer-based self-supervised learning framework that provides versatile feature extraction for both classification and segmentation tasks across different CT scan types.
- We propose a novel training technique, developed to train a DINO model for targeted tasks by guiding it to capture highly specific features in its generated representations. This approach enhances the model's ability to focus on relevant characteristics within the data by leveraging label guidance to direct its attention.
- Our proposed system seamlessly integrates self-supervised learning (DINO-LG), classification, and segmentation models to deliver a fully automated coronary calcium scoring solution, which reduces manual analysis requirements and enables consistent and efficient CAC assessment.

2. Related Work

Recent reviews has highlighted notable advances in CAC scoring and segmentation facilitated by artificial intelligence (AI) techniques [23, 24, 25, 26, 27]. The integration of AI in quantifying CAC on CT scans presents a transformative approach to cardiovascular risk assessment. An FDA-approved deep learning (DL) algorithm (NANOX AI) in a single-center retrospective study to measure CAC on non-contrast ECG-non-gated chest CT is used [28]. As a result of the analysis of 527 patient data, the interpretation by cardiologists showed an 88.76% agreement with the AI classification. On non-gated images, DL-based CAC scoring software reported using chest CT scans [29]. When assessing the agreement of scores based on CAC groups all intraclass correlation coefficients (ICCs) were good enough. Sartorette et al. [30] evaluated CAC scoring by a fully automated DL-based tool (AVIEW CAC, Coreline Soft). The similarity between the CAC ground truth values and the results obtained from the DL model was 0.986. in the studies performed on the CT data obtained for 56 patients included in the analysis. In another study by Assen et al. [9], the coronary calcium volume on non-contrast cardiac CT was obtained using a DL based algorithm (AI-Rad Companion Chest CT, Siemens Healthineers, Forchheim, Germany). The Agatston score obtained as a result of the studies and the calcium volume determined by AI show a high correlation with a correlation coefficient of 0.921. These studies, performed using software produced by specialized companies, have shown that rapid and precise assessment of CAC can facilitate the practical application in routine CT data, providing an important contribution on how patients with different risks should be treated.

A novel DL model is developed by Eng et al. [31] to automate CAC scoring, demonstrating high accuracy and speed on both dedicated gated coronary CTs and non-gated chest CTs. For detecting CAC, the algorithm provided a sensitivity of 71% to 94% and a positive predictive value of 88% to 100% across four different datasets. Velzen et al. [32] evaluated the effectiveness of a deep learning method for CAC scoring across different types of CT examinations to see if the algorithm result well when trained with representative images from different CT protocols. At baseline, the DL algorithm achieved intraclass correlation coefficients (ICCs) of 0.79-0.97 for CAC, which improved to 0.85-0.99 with combined training. Later, Zeleznik et al. [33] introduced a deep learning system capable of accurately predicting cardiovascular events by quantifying coronary calcium, validated in a diverse population of 20,084 individuals on various routine cardiac-gated and non-gated CT. The study found a very high correlation of 0.92 ($P < 0.0001$) and substantial agreement between the automated and manual calculations of calcium risk groups. These studies highlight the increasing role of DL in improving clinical decision making in CAC detection. Peng et al. [34] used a DL algorithm to quantify CAC on non-gated CT for association with cardiovascular outcomes. After adjusting for various demographic and clinical factors, individuals with DL-CAC scores of 100 or more showed a notably increased

risk of all-cause mortality, as well as higher risks for composite outcomes involving myocardial infarction and stroke.

Active multitask learning with uncertainty-weighted loss is proposed by Follmer et al. [35] for CAC scoring in ECG-gated CT. The proposed model was tested on a total of 1,275 patient data consisting of a combination of three different datasets, and the results obtained showed a strong agreement with clinical outcomes ranging from 0.80 to 0.97. A 3D deep convolutional neural network (CNN) model is trained for Agatston scores using a database of 5973 non-contrast non-ECG gated chest CT without a prior segmentation of the CACs [36]. This model achieved a Pearson correlation coefficient of $r = 0.93$; $p \leq 0.0001$ when compared with ground truth data. In another study, Ihsdayhid et al. [37] proposed fully automated DL model to detect and measure CAC scores on ECG-gated CTs. The CAC score results from the automated model showed a strong correlation with the reference standard, indicated by a Spearman's correlation of $r=0.90$ and an ICC of 0.98. An automatic deep learning approach [37] on 365 patients was developed to quantify CAC scores. The designed model was tested on an unseen cohort of 240 patients, and the results indicate that the model can effectively quantify CAC and classify risk in CT angiography. One of the studies using the public Coronary Calcium and chest CT's (COCA) dataset proposed a novel semantic-prompt scoring siamese network [38], while the other study proposed a lightweight 3D convolutions [39] with less memory requirements. The results obtained from these studies show that deep learning can produce similar results to the methods in the current literature in CAC scoring.

There have been studies using U-Net architecture [40], a convolutional neural network designed for efficient image segmentation, to automate the measurement of CAC from CT scans. This novel approach addresses the drawbacks of conventional manual scoring methods, which can be labor-intensive and require specialized knowledge. Gogin et al. [41] evaluated 3D U-Net model to automatically estimate the amount of CAC on a database of 783 CT examinations and the final model resulted in a C-index of 0.951 on the test set. Bujny et al. [42] introduced an algorithm for segmenting coronary arteries in multi-vendor ECG-gated non-contrast cardiac CT images, leveraging a new framework for semi-automatic Ground Truth (GT) creation through image registration. The model achieved a Dice coefficient of 0.65 ± 0.08 for segmenting coronary arteries, evaluated against manually registered test GT. [43] et al. proposed a DL approach for the detection of CAC on both non-contrast and contrast-enhanced CT scans, involving 295 consecutive CT scans, and demonstrated significant agreement with manual assessment (Cohen's Kappa=0.61, Bland-Altman mean difference=-40.8mm³). Contributing to the success of the U-net architecture, the Heart-labeling method was further enhanced to provide fully automated total and vessel-specific CAC quantification [44]. 560 gated CT images were used to train the model and the overall accuracy for CAC classification was obtained with Cohen's kappa $k = 0.89$ and 0.95 for validation and testing, respectively. Zhang et al. used

a multi-task DL framework to train the U-Net-based model on 232 non-contrast cardiac-gated CT scans [45]. The average Agatston score for the automatic method was 535.3, while the manual method had an average of 542.0 ($P = 0.993$). Likewise, the calcium volume score was 454.2 for the automatic method and 460.6 for the manual method ($P = 0.990$).

In another study [46], the model was trained using focal loss, a modified version of cross entropy loss that emphasizes challenging samples by decreasing the weight of those that are easier to classify. A retrospective study of 1,811 retrospectively collected CT data showed that U-Net++ significantly outperformed U-Net with accuracies ranging from 0.8 to 1.0. Since non-gated CTs are more commonly performed, [47] et al. developed a semi-supervised U-Net model to accurately assess risk in these scans, having been trained on gated scans from the before being applied to the non-gated images. The performance of the model showed a 91% improvement in mean absolute error (with gated scans at 62.38 and non-gated scans at 674.19) and a 32% increase in F1-score (gated scans at 0.68 compared to non-gated scans at 0.58). By effectively identifying and segmenting calcium deposition areas, the U-Net model improves both the speed and accuracy of CAC scoring, making it a useful tool for assessing cardiovascular risk. Its versatility across different imaging protocols and strong alignment with expert evaluations demonstrate its potential for broad clinical use, ultimately leading to earlier interventions and better patient outcomes in cardiovascular health.

Recently, in addition to traditional supervised learning methods, self-supervised learning (SSL) techniques use tasks that replace traditional labels with features extracted from the input data, allowing the model to learn data representations without requiring explicit supervised labels [48, 22, 49]. This approach is particularly valuable for large-scale medical data, where labeling image data is often costly and time consuming. Shakouri et al. [50] highlighted the effectiveness of SSL, DINO, based on a vision transformer in enhancing chest X-ray classification. A quantitative analysis shows that the proposed method surpasses state-of-the-art techniques in accuracy and achieves similar performance in terms of AUC and F1-score, while requiring significantly less labeled data. Matsoukas et al. [51] demonstrated the advantages of SSL dealing with different scenarios. Through experimental studies, they showed that vision transformers can effectively replace CNNs for medical 2D image classification when appropriate training protocols are implemented. Additionally, Pérez-García et al. [52] explored SSL and introduced RAD-DINO, a biomedical image encoder pre-trained solely on diverse biomedical imaging data. Baharoon et al. [53] developed foundational models for the medical field, using DINOv2 to benchmark disease classification and organ segmentation. Experimental studies have shown the potential to alleviate the problem of data annotation while improving model generalizability and robustness. Huang et al. [54] performed a glioma grading task and comprehensive analysis of DINOv2 and ImageNet pre-trained models using three clinical modalities

of brain MRI data. DINOv2 outperformed other models, especially when taking advantage of the frozen mechanism.

3. Methodology

3.1. Overall Architecture

The proposed architecture for CAC scoring is presented in Fig. 1. The overall architecture for coronary calcium detection and scoring combines self-supervised learning (via the DINO model) with segmentation techniques to precisely identify calcified regions in CT scan slices. The process begins with a complete CT scan, which is divided into smaller patches. These patches are fed into a Vision Transformer (ViT) backbone as part of the DINO model, where each patch undergoes linear projection to extract meaningful features. The length and size of the features are generated by DINO model can vary depending on the number of heads utilized in multi-head attention. The embedded features introduced by the DINO model incorporate distinguishable characteristics for each CT slice, depending on whether it contains calcification or not.

In the second step, the extracted features from DINO model are fed into to a transformers-based binary classification model to classify CT slices as either containing calcified areas or not. CT slices with a high probability of calcification are sent to a pre-trained U-Net model to segment the calcified regions, calculating the total CAC score for the case in the final step. This combined approach allows for both classification and detailed segmentation of calcified areas, enabling more accurate coronary calcium detection and quantification.

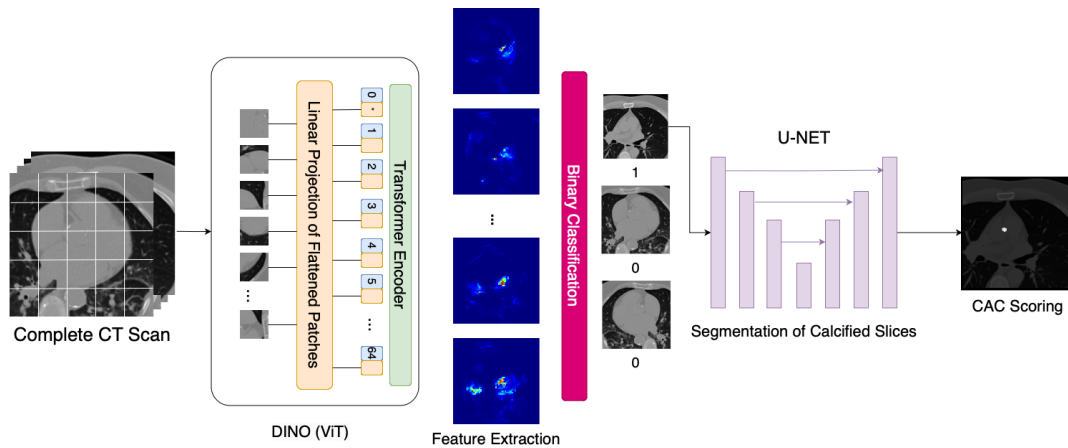


Figure 1: The illustration of overall architecture for detection of calcified CT slices. Visualized features are representative.

3.2. Label-Guided Data Augmentation and DINO Training

Data Augmentation. Data augmentation techniques are key components for self-supervised learning to enhance model's robustness and improve generalizable representations by identifying the underlying features. The most well-known augmentation techniques include random cropping, random flipping, random rotating, and color jittering [55].

Recent studies, especially using medical images such as CT scans, do not utilize data augmentation techniques like solarization and color jitter, as these are not suitable for processing medical images [56]. Instead, alternative data augmentation techniques are utilized like additional noise and brightness changing. Table 1 shows the most common data augmentation techniques used for medical images and compares them with the augmentation techniques used in the traditional DINO model [57]. In our approach, we apply the medical data augmentation techniques as outlined in the table.

Table 1

Comparison of augmentation techniques utilized for RGB images and medical images

Augmentation Tech.	RGB Images	Medical Images
Random Horizontal Flip	✓	✓
Random Vertical Flip	✓	✓
Random Crop	✓	✓
Random Resized Crop	✓	✓
Gaussian Blur	✓	✓
Solarization	✓	✗
Color Jitter	✓	✗
Brightness Changing	✗	✓
Noise Addition	✗	✓

Label-Guided Data Augmentation. Random data augmentation techniques have a reputation on increasing overall accuracy and they are useful techniques to cope with imbalanced and insufficient data for training. In particular, the random cropping enhancement technique is observed to make a significant performance improvement on classification tasks. For specific tasks and including a limited dataset, trained models are likely to generate suitable outputs as expected [58].

However, random augmentation techniques are useful for specific tasks, and the significant growth in dataset leads the model generating more generalized outputs and representations. In particular, models trained with self-supervised learning techniques tend to generate more generalized representations, leading to a dramatic performance decrease in specific tasks [59]. Additionally, a generalized model achieving desired

results requires more resources and time, when it is compared to the other models that are trained with smaller datasets.

In general, DINO training approach, it is provided as an option to choose the number of augmentation count, which determines how many random cropping are extracted from the images introduced to the model. Especially, the parameter for number of random local cropping has a crucial role for specifying the number of local cropping, having ratio between 0.05 and 0.4 to the introduced image. These random local cropping occupies majority of augmentation process and are important to generate generalized representations. Although these local random captures important features, it is required more time for randomized cropping including desired local areas in the image. To make an efficient training and generating random local cropping focusing on targeted areas such as calcified ROIs, we introduce Label-guided data augmentation technique.

Label-guided data augmentation uses the parameter of the number of random local cropping and applies the random augmented cropping with the same amount of this parameter, such as it is applied in the traditional approach. Addition to this random augmentation, our technique also checks the corresponding labels to the introduced images. Existing labels corresponding to the images represented to the model are used to force the model learning specific local features by generating cropping according to the labels. A simple representation of label-guided data augmentation is depicted in Fig. 2. In addition to these extracted label-guided random local cropping, medical augmentation techniques are applied on these locally cropped features, which are listed in Table 1.

First step in label-guided data augmentation is choosing a random coordinate from the labels. This random pixel identifies the focusing center for guided augmentations. By randomly selecting pixel coordinates from labels and applying augmentations, the model is forced to focus on specific regions, preventing it from learning unnecessary local features.

The next step involves determining the frequency of label-guided augmentations. This parameter significantly impacts the model's focus on Region of Interests (ROIs) corresponding to labels. A DINO model heavily reliant on label-guided augmentations generates representations strongly capturing labeled area features. However, this imbalance can lead to the neglect of other useful features. To preserve both labeled and unlabeled feature information, a small amount of label-guided augmentation is sufficient. In our experiments, we found an optimal balance of 33% label-guided augmentations within total local augmentations. Considering that labeled images typically constitute less than 10% of the trough dataset, label-guided augmentations are applied relatively infrequently during training.

The Fig. 3 represents locally guided data augmentation on a CT slice which includes a calcification. In our experiments, random local data augmentation was set to 4, while guided local data augmentation was set to 12, in order to preserve the

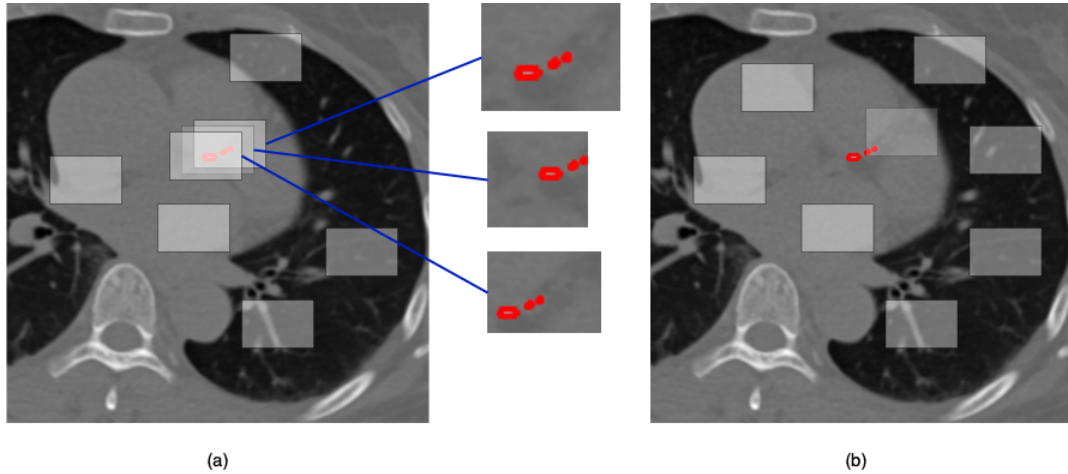


Figure 2: Representation for label guided augmentation, focusing on specific ROIs and generating more than one cropping for calcified regions (a). Completely random local image cropping is utilized by standard DINO training (b).

randomness of the local data augmentation process. To illustrate the contributions of guided data augmentation, Fig. 4 presents a visualization of the outputs from the self-attention heads of DINO models trained using both label-guided and standard methods.

3.3. Binary Classification of DINO Features

The features are generated by DINO model is extracted from the last layer of multi-head self attention modules. The size of the extracted feature's length is equal to the size of the embedded dimensions which depends on the selected ViT model. In this study, we focused on generating a diverse set of features to capture small details, such as calcified areas in CT slices. These features are differentiable by using a discriminative method, such as classifiers. To achieve accurate classification of CT slices containing calcified areas, we utilize a linear classification model that has trained the generated features by DINO model.

3.4. Segmentation and Calcium Scoring

The next step after the classification task is the segmentation of chosen CT slices as calcified. As it is mentioned in recent studies, segmentation of calcified areas has a high accuracy rate in a case of CT slices known to have calcification. If it is considered that CNN based architectures have lack of focusing on global features and require improvements to enhance their distinctive capabilities, it is understandable why recent studies do not include uncategorized cases in their own study.

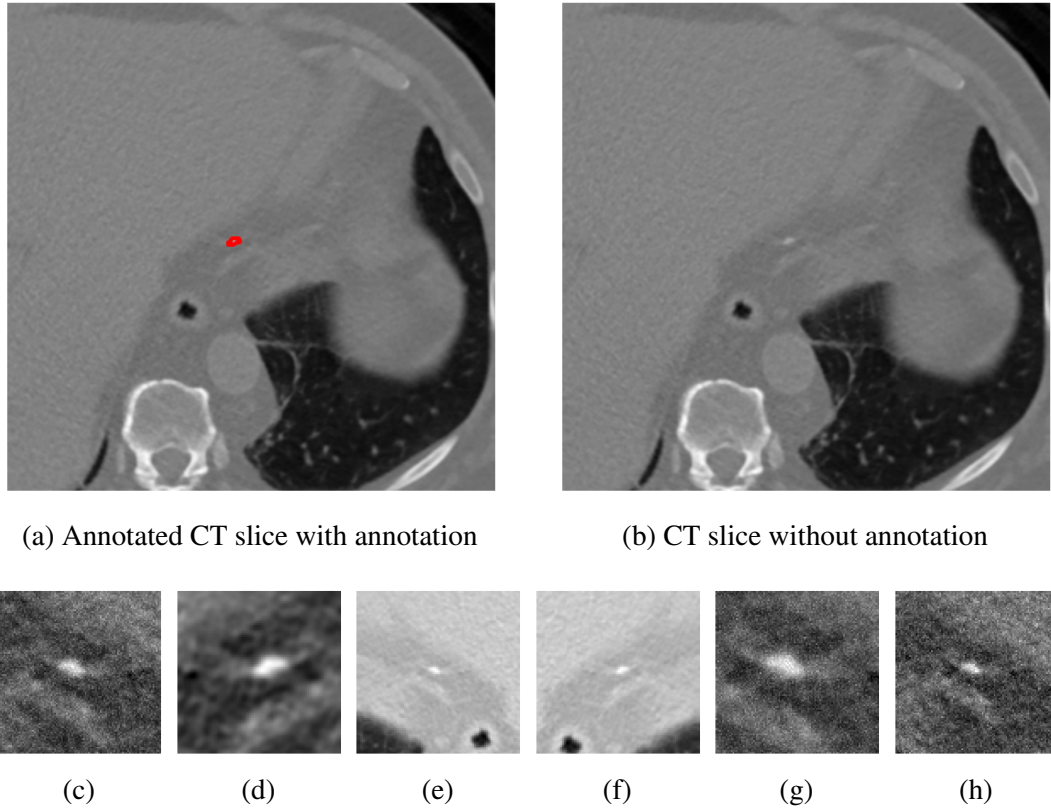


Figure 3: Representation of guided local data augmentation. Figure *a* represents labeled CT slice, while *b* represents the same image without annotation. The figures from *c* to *h* shows the guided local data augmentations utilized in DINO training.

Despite this, even though our segmentation task yields results comparable to recent studies, our proposed architecture makes it possible to work it with unrelated cases and images.

4. Experiments and Results

4.1. Experimental Setup

The experimental setup consists of three steps of model training; starting with DINO model training, followed by the classification model, and finally training a U-NET for segmentation and CAC scoring. All experiments are performed on a single node with 8 H100 GPUs.

Dataset. In this study, we utilized the COCA- Coronary Calcium and Chest CT dataset, collected by Stanford Hospital and Clinics, to assess calcium deposition in the coronary arteries, which can be accessed at [60]. This dataset comprises images from computed tomography (CT) scans used for evaluating coronary calcium scores. It includes gated coronary CTs with corresponding segmentation scores and paired gated

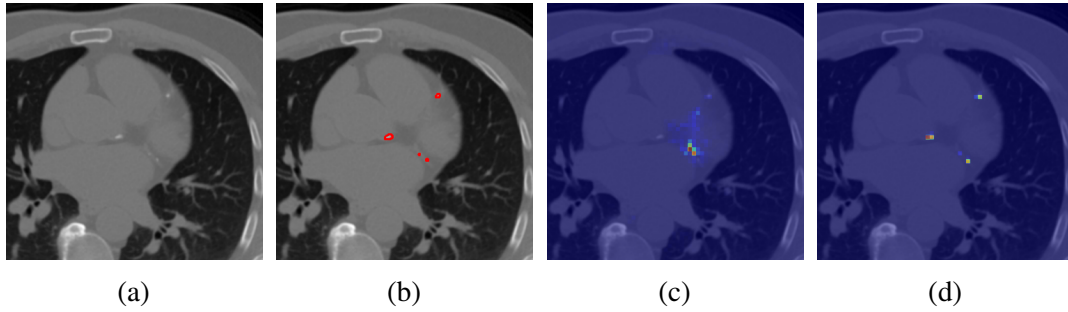


Figure 4: Representation of generated features by DINO-LG model trained with label-guided approach and standard DINO training. Figure (a) represents a CT slice having calcified area and (b) shows annotated area for calcification. Figure (c) and (d) represent visualization of overlay self-attention maps are generated by standard DINO model and DINO-LG model, respectively.

and non-gated routine chest CTs. Gated scans are less frequently employed in clinical practice since they are typically dedicated to specific tasks like detecting calcification, whereas non-gated scans are more versatile and serve multiple diagnostic purposes.

A total of 789 patients underwent retrospective gated coronary CT scans, resulting in 789 scans. These gated scans include masked segmentations for the entire 3D volume. In addition, 214 patients had retrospective non-gated coronary CT scans containing coronary artery calcium (CAC) scores stored in an XML file. Each CT volume in the dataset has a consistent width and height of 512 pixels, while the number of slices varies, maintaining a constant slice thickness of 3 mm. The gated dataset contains 36,411 images, of which 3,656 contain at least one CAC object classified into one of four coronary arteries. In total, there are 6,211 calcified objects with an average size of 119 pixels, representing approximately 0.04% of each image. All CT scans are saved as DICOM files.

In our experiments, CT scans are included in dataset chosen from the patients with annotations, and they were split into training, validation, and test sets based on the total calcium score distribution of the patients, ensuring balanced datasets from cases with annotations. Additionally, a separate dataset was created for training the DINO-LG model, including all gated and non-gated CT scans while excluding patients from the validation and test sets. The distribution of patients across the training, validation, and test datasets, along with their respective risk scores, is detailed in Table 2.

DINO Training. The original DINO repository provides sufficient guidance for training the DINO model on both single and multiple GPU setups. In our experiments, the same dataset is used to train two versions of the DINO model: the first using our label-guided training approach, and the second following the standard DINO training with data augmentations as described in Table 1. In addition to the hyper-parameters provided in the DINO repository such as the number of random local cropping (RLC),

Table 2

Patient Counts by Risk Category and Agatston Score Range for Train, Validation, and Test Sets

Risk Category	Range (Agatston Score)	Train Set	Validation Set	Test Set
Low Risk	0-10	45	5	6
Moderate Risk	11-100	117	15	15
High Risk	101-400	98	12	12
Very High Risk	>400	94	12	12
Total Patients		354	44	45

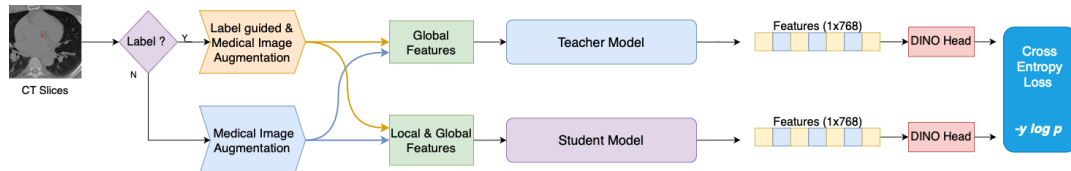
Table 3

Comparison of hyper-parameters for Label-Guided DINO model (DINO-LG) and DINO model

Model Name	ViT Type	RLC	GLC	Augmentation	# Epochs
DINO	ViTb8	16	0	Medical	150
DINO-LG	ViTb8	12	4	Medical	150

we have defined an additional hyper-parameter for our proposed method, referred to as the number of guided local cropping (GLC) given in Table 3.

A simplified representation of the label-guided training for DINO-LG model is shown in Figure 5. The main difference from traditional DINO model training is the integration of label checks for the corresponding CT slices. CT slices having labels or calcified areas undergo using our proposed label-guidance augmentation approach. Conversely, the remaining CT slices without calcification are augmented with the standard DINO model's hyper-parameters, with medically appropriate augmentation techniques as outlined in Table 1.

**Figure 5:** The illustration of training DINO-LG model.

Training Classifier. The features generated by the DINO model are presented as input to the classification model to detect CT slices including calcified areas for each chest CT scans. It is also expected from the classification model to distinguish CT slices that are irrelevant to calcified areas. This is a crucial process to determine

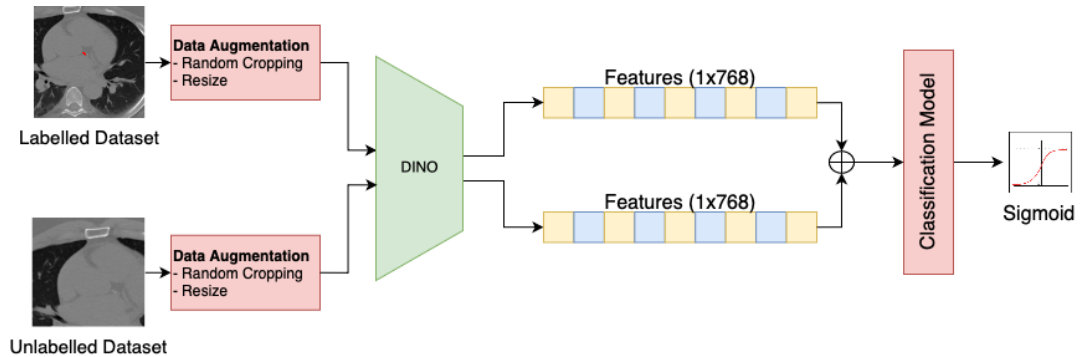
Table 4

Hyper-parameters for U-NET based segmentation models.

Model Name	# Initial Filter	Image Size	Batch Size	LR	# Epochs
U-NET	64	512x512	64	1e-4	100
Attention U-NET	64	512x512	64	1e-4	100
Swin U-NET	64	512x512	64	1e-4	100

whether the features generated by the DINO model include calcified areas, even if these slices are not related to the chest or calcified areas.

The classifier model is trained with the training dataset which is extracted from COCA dataset according to the distribution of calcification scores. As explained in the dataset section, the training dataset includes the complete CT scans corresponding to each patient ID. The ratio of annotated CT slices to the complete CT scans is 15%. Despite this imbalance, augmentation techniques such as random cropping and resizing are applied to the CT slices to enhance model robustness. For training, the dataset is further split into two subsets: labeled and unlabeled datasets, extracted from the training dataset. The labeled dataset consists of annotated CT slices, while the unlabeled dataset contains non-annotated slices, enabling the model to learn from both calcified and non-calcified areas. The core architecture for training and implementing the classification model is illustrated in Figure 6.

**Figure 6:** The illustration of training classifier model.

Training Segmentation Model. The segmentation models used in our experiments are based on U-NET-like architectures, using the same datasets and training techniques applied as in the classification task. The architectures we implemented include U-NET, Attention U-NET, and Swin U-NET, and their configurations are detailed in Table 4.

Table 5

Comparison of Performance Metrics of Classification Task: Standard DINO vs. DINO-LG

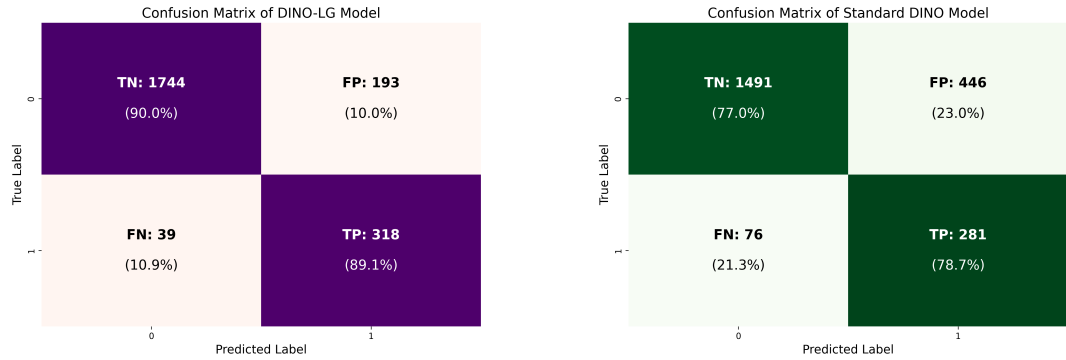
Metric	Standard DINO	DINO-LG
Confusion Matrix		
True Negatives (TN)	1491	1744
False Positives (FP)	446	193
False Negatives (FN)	76	39
True Positives (TP)	281	318
Classification Metrics		
Class 0 Precision	0.95	0.98
Class 0 Recall	0.77	0.90
Class 0 F1-score	0.85	0.94
Class 1 Precision	0.39	0.62
Class 1 Recall	0.79	0.89
Class 1 F1-score	0.52	0.73
Accuracy	0.77	0.90
Sensitivity and Specificity		
Sensitivity (True Positive Rate)	0.79	0.89
Specificity (True Negative Rate)	0.77	0.90

4.2. Performance Analysis of DINO and Segmentation Models

Comparison of DINO-LG and DINO model via Classification. The comparison is conducted on two different models trained with our label-guided approach and standard DINO model. The confusion matrix for both models are represented in Figure 7 and includes TP (True-Positive), TN (True-Negative), FP (False-Positive) and FN (False-Negative) predictions. The linear classification model is trained for 10 epochs, because of the increase in FN predictions. FN predictions indicate that the predicted slices containing calcified areas were incorrectly classified as unannotated or without calcification. Thus, it is crucial keeping FN predictions in low weighted in among other predictions.

The other important prediction type, FP predictions indicate that the slices annotated as non-calcified areas were incorrectly classified as containing calcified areas. Although FP predictions are significantly higher than FN predictions across all predicted slices, it should be noted that segmentation models do not consider FP slices if they do not contain missed or unnoticeable calcified areas. The remaining prediction types of TP and TN represent the slices that were correctly predicted as containing calcified areas and non-calcified areas. The confusion matrix provided

for both models reveals that the DINO-LG model has a significant improvement in the prediction of TN and FN. This also demonstrates that the DINO model can be effectively trained for specific tasks.



(a) F1-score of the guided classification model.

(b) F1-score of the non-guided classification model.

Figure 7: Classification results showing the F1-score for both DINO model trained with label-guided approach (a) and standard approach (b).

Table 5 presents a comparative analysis of the classification performance metrics for the Standard DINO model and the proposed DINO-LG model. The DINO-LG model demonstrates substantial improvements across all evaluated metrics. In the confusion matrix, DINO-LG achieves a notable reduction in both False Positives (193 vs. 446) and False Negatives (39 vs. 76), resulting in higher True Positives (318 vs. 281) and True Negatives (1744 vs. 1491). These improvements translate into better classification metrics; for Class 0, the precision improves from 0.95 to 0.98, recall increases from 0.77 to 0.90, and the F1-score rises from 0.85 to 0.94. Similarly, for Class 1, precision improves from 0.39 to 0.62, recall increases from 0.79 to 0.89, and the F1-score rises from 0.52 to 0.73.

The overall accuracy of DINO-LG (0.90) significantly outperforms Standard DINO (0.77), highlighting its effectiveness in distinguishing between calcified and non-calcified slices. Furthermore, the sensitivity (True Positive Rate) and specificity (True Negative Rate) of DINO-LG improve to 0.89 and 0.90, respectively, compared to 0.79 and 0.77 for the Standard DINO model. These enhancements demonstrate the superior ability of the DINO-LG model to identify calcification while reducing false classifications, thereby ensuring more reliable and clinically relevant predictions.

Segmentation Experiments The segmentation models were tested on the same dataset used in the classification experiments, independently of the classification model. Before integrating the segmentation model with DINO features, this section evaluates U-NET-based architectures to determine their suitability for combination

Table 6

IoU and Dice scores for RCA, LAD, LCA, and LCX classes across three U-NET based segmentation models on the Test Dataset.

Model Name	RCA		LAD		LCA		LCX	
	IoU	Dice	IoU	Dice	IoU	Dice	IoU	Dice
Attention U-NET	0.95	0.92	0.63	0.77	0.36	0.53	0.59	0.74
Swin U-NET	0.96	0.96	0.52	0.68	0.10	0.16	0.35	0.52
U-NET	0.97	0.98	0.61	0.75	0.43	0.60	0.49	0.70

with the DINO model in the main structure. The performance of U-NET-based models is presented in Table 6. As shown in the table, the basic U-NET and Attention U-NET architectures achieved significantly higher scores across all coronary artery classes: RCA (Right Coronary Artery), LAD (Left Anterior Descending), LCA (Left Coronary Artery), and LCX (Left Circumflex).

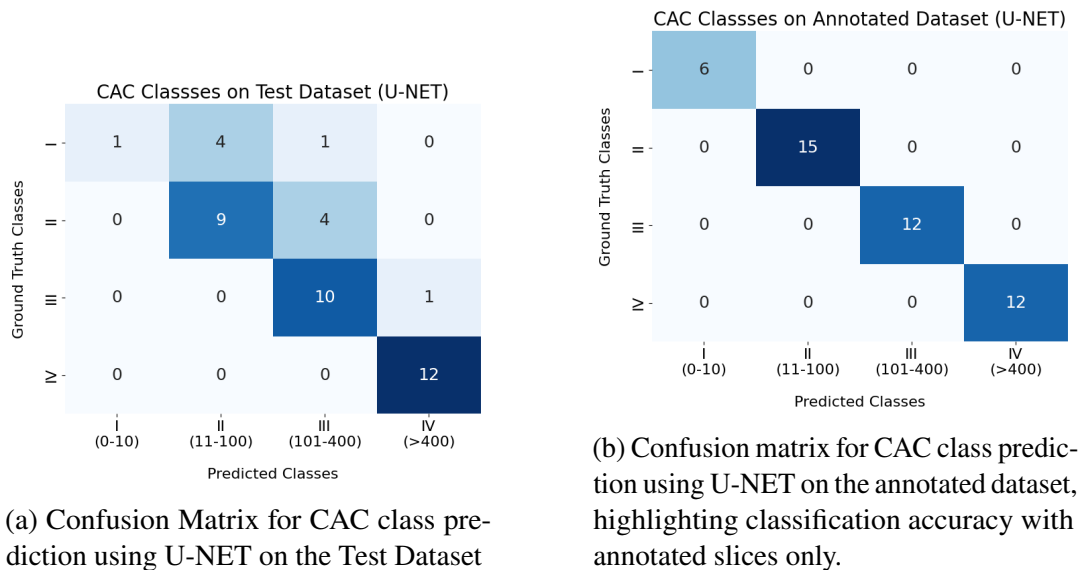


Figure 8: CAC class predictions for each patient in the test dataset using U-NET.

The U-NET architecture performs well in identifying high risk calcification areas but encounters challenges with smaller calcified regions in CT slices. The lack of annotations for many CT slices often leads the model to incorrectly segment unannotated areas, significantly impacting F1-scores due to potential mislabeling. The CAC scoring results produced by the U-NET architecture are shown in Figure 8a, while Figure 8b illustrates the CAC classification results using the annotated dataset.

Table 7

Comparison of classification performance metrics between UNET and Our Approach models across RCA, LAD, LCA, and LCX classes.

Metric	UNET			Our Approach		
	Precision	Recall	F1-score	Precision	Recall	F1-score
RCA	1.00	1.00	1.00	1.00	1.00	1.00
LAD	0.68	0.86	0.76	0.83	0.86	0.85
LCA	0.62	0.59	0.60	0.71	0.59	0.64
LCX	0.70	0.79	0.75	0.81	0.79	0.80
Avg. Accuracy	0.75	0.81	0.78	0.84	0.81	0.82

The discrepancies between these results indicate that CT slices without calcified areas have a negative impact on the overall classification performance.

4.3. Performance Results of the Integrated System

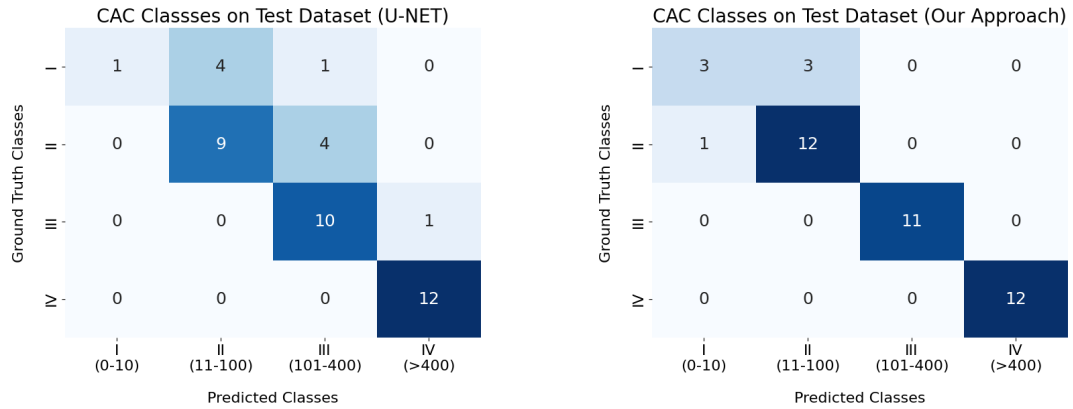
The integrated system, combining DINO-LG based feature extraction, classification and U-NET segmentation, demonstrates significant improvement in identifying and scoring coronary artery calcification. In the classification part, the DINO-LG model efficiently distinguishes CT slices whether having calcified areas or not, ensuring that only relevant images are forwarded to the segmentation model. Identifying CT slices containing calcified areas has a crucial role to leverage segmentation task as it represented in Figure 8.

The segmentation model used in the system is U-NET, chosen for its superior performance in IoU and Dice scores. A comparative analysis of the segmentation performance on the test dataset is conducted between the standalone U-NET and the integrated U-NET used within the system. The results, presented in Table 7, detail performance across four distinct classes: RCA, LAD, LCA, and LCX.

For the RCA class, both methods generate perfect scores and able to segment calcified areas in the RCA perfectly. However, our approach excels particularly in the LAD and LCX categories, with a notable 0.85 F1-score in LAD and 0.80 in LCX, compared to the lower scores achieved by the standalone U-NET. The average accuracy of the integrated approach is also higher at 0.84 compared to U-NET's 0.75, suggesting that the additional feature extraction via DINO-LG plays a significant role in enhancing classification reliability. These results validate the effectiveness of the integrated system in precisely localizing and quantifying calcifications, especially in more challenging regions such as LAD and LCX.

The segmentation results generated by standalone U-NET and our system are also utilized for calculating CAC scores which are subsequently categorized into risk

DINO-LG: A Task-Specific DINO Model For Coronary Calcium Scoring



(a) Confusion Matrix for CAC Prediction using standalone U-NET

(b) Confusion Matrix for CAC Prediction using our proposed system

Figure 9: Confusion matrices showing improved CAC classification accuracy of our proposed DINO-LG integrated system (b) compared to the standalone U-NET model (a) on the test dataset.

classes based on these scores. As it is illustrated in Figure 9, our proposed system demonstrates a more refined classification performance compared to the standalone U-NET, especially in distinguishing between moderate and high risk classes.

The comparative results presented in Table 8 clearly demonstrate the superiority of our integrated system over the standalone U-NET model in coronary artery calcium (CAC) scoring. Our integrated system achieves consistent improvements across all risk categories, particularly excelling in precision, recall, and F1-scores for both low-risk and high-risk categories. For instance, in the "Low Risk" category, precision, recall, and F1-score all reach perfect values of 1.00 in the proposed system, whereas the U-NET model struggles with a precision of 0.67 and F1-score of 0.77.

Sensitivity and specificity metrics further underline the system's effectiveness. Average sensitivity (TPR) across all risk categories rises from 0.69 in the U-NET model to 0.86 in the proposed system, demonstrating improved detection of calcified areas. Similarly, specificity (TNR) increases from 0.92 to 0.97, reducing false positives and enhancing the model's reliability.

Moreover, the overall weighted averages for precision, recall, and F1-score in our approach are 0.90 each, substantially outperforming the corresponding values of 0.80, 0.76, and 0.73 in the U-NET model. These advancements signify a robust and efficient framework, ensuring accurate classification and segmentation of calcifications while minimizing false negatives and false positives. This enhanced performance is particularly beneficial in clinical settings, where accurate CAC assessment directly impacts patient management and treatment outcomes.

Table 8

Comparison of classification performance metrics for U-NET and Our System on CAC scoring.

Metric	U-NET	Our Approach
Low Risk Metrics (0-10)		
Precision	0.67	1.00
Recall	0.91	1.00
F1-score	0.77	1.00
Sensitivity (TPR)	0.17	0.50
Specificity (TNR)	1.00	0.97
Moderate Risk Metrics (11-100)		
Precision	1.00	0.75
Recall	0.17	0.50
F1-score	0.29	0.60
Sensitivity (TPR)	0.69	0.92
Specificity (TNR)	0.86	0.90
High Risk Metrics (101-400)		
Precision	0.69	0.80
Recall	0.69	0.92
F1-score	0.69	0.86
Sensitivity (TPR)	0.91	1.00
Specificity (TNR)	0.84	1.00
Very High Risk Metrics (> 400)		
Precision	0.92	1.00
Recall	1.00	1.00
F1-score	0.96	1.00
Sensitivity (TPR)	1.00	1.00
Specificity (TNR)	0.97	1.00
Overall Metrics		
Accuracy	0.76	0.90
Weighted Avg Precision	0.80	0.90
Weighted Avg Recall	0.76	0.90
Weighted Avg F1-score	0.73	0.90
Average Sensitivity (TPR)	0.69	0.86
Average Specificity (TNR)	0.92	0.97

5. Discussion and Conclusion

In this paper, we propose a novel approach to train DINO, vision foundational model, with the guidance of existing labels or annotations. The proposed label-guided training approach encourages the model highlighting and paying more attention to the annotated areas. We show effectiveness of this approach on coronary calcium detection and scoring, by integrating a classification head and segmentation model

to DINO-LG model. Experiments reveal that, DINO-LG model is able to identify calcified areas on CT slices when guided to focus on annotated regions during training.

The training method we propose for the DINO model is not limited to a specific application, such as coronary artery calcium detection. This approach can be applied to various datasets with annotations for lungs, liver, tumors, and other regions, especially considering that foundational vision models can focus on multiple features simultaneously. Additionally, training a foundational model across multiple fields can enhance its ability to capture a wider range of distinctive features.

6. Acknowledgements

The project described was supported by the NIH National Center for Advancing Translational Sciences through grant number UL1TR001998. The content is solely the responsibility of the authors and does not necessarily represent the official views of the NIH. We thank the Scientific and Technological Research Council of Türkiye (TUBITAK) for supporting the author Caner Ozcan through BIDEB-2219 International Postdoctoral Research Fellowship Program (grant no. 1059B192300232).

References

- [1] World Health Organization. Cardiovascular diseases (CVDs). in World Health Organization, vol. 2021., 2021.
- [2] National Center for Health Statistics. National center for health statistics. Multiple Cause of Death 2018–2022 on CDC WONDER Database. Accessed May 3, 2024. <https://wonder.cdc.gov/mcd.html>, 2024.
- [3] Connie W Tsao, Aaron W Aday, Zaid I Almarzooq, Cheryl A M Anderson, Pankaj Arora, Christy L Avery, Carissa M Baker-Smith, Andrea Z Beaton, Amelia K Boehme, Alfred E Buxton, Yvonne Commodore-Mensah, Mitchell S V Elkind, Kelly R Evenson, Chete Eze-Nliam, Setri Fugar, Giuliano Generoso, Debra G Heard, Swapnil Hiremath, Jennifer E Ho, Rizwan Kalani, Dhruv S Kazi, Darae Ko, Deborah A Levine, Junxiu Liu, Jun Ma, Jared W Magnani, Erin D Michos, Michael E Mussolino, Sankar D Navaneethan, Nisha I Parikh, Remy Poudel, Mary Rezk-Hanna, Gregory A Roth, Nilay S Shah, Marie-Pierre St-Onge, Evan L Thacker, Salim S Virani, Jenifer H Voeks, Nae-Yuh Wang, Nathan D Wong, Sally S Wong, Kristine Yaffe, Seth S Martin, and American Heart Association Council on Epidemiology and Prevention Statistics Committee and Stroke Statistics Subcommittee. Heart disease and stroke statistics-2023 update: A report from the american heart association. *Circulation*, 147(8):e93–e621, February 2023.
- [4] Juhani Knuuti, William Wijns, Antti Saraste, Davide Capodanno, Emanuele Barbato, Christian Funck-Brentano, Eva Prescott, Robert F Storey, Christi Deaton, Thomas Cuisset, Stefan Agewall, Kenneth Dickstein, Thor Edvardsen, Javier Escaned, Bernard J Gersh, Pavel Svitol, Martine Gilard, David Hasdai, Robert Hatala, Felix Mahfoud, Josep Masip, Claudio Muneretto, Marco Valgimigli, Stephan Achenbach, Jeroen J Bax, and ESC Scientific Document Group. 2019 ESC guidelines for the diagnosis and management of chronic coronary syndromes. *Eur. Heart J.*, 41(3):407–477, January 2020.
- [5] Matthijs Oudkerk, Arthur E Stillman, Sandra S Halliburton, Willi A Kalender, Stefan Möhlenkamp, Cynthia H McCollough, Rozemarijn Vliegenthart, Leslee J Shaw, William Stanford, Allen J Taylor, Peter M A van Ooijen, Lewis Wexler, Paolo Raggi, European Society of Cardiac Radiology, and North American Society for Cardiovascular Imaging. Coronary artery calcium screening: current status and recommendations from the european society of cardiac radiology and north american society for cardiovascular imaging. *Eur. Radiol.*, 18(12):2785–2807, December 2008.
- [6] A S Agatston, W R Janowitz, F J Hildner, N R Zusmer, M Viamonte, Jr, and R Detrano. Quantification of coronary artery calcium using ultrafast computed tomography. *J. Am. Coll. Cardiol.*, 15(4):827–832, March 1990.
- [7] Harvey S Hecht. Coronary artery calcium scanning: past, present, and future. *JACC Cardiovasc. Imaging*, 8(5):579–596, May 2015.
- [8] David Eng, Christopher Chute, Nishith Khandwala, Pranav Rajpurkar, Jin Long, Sam Shleifer, Mohamed H Khalaf, Alexander T Sandhu, Fatima Rodriguez, David J Maron, Saeed Seyyedi, Daniele Marin, Ilana Golub, Matthew Budoff, Felipe Kitamura, Marcelo Straus Takahashi, Ross W Filice, Rajesh Shah, John Mongan, Kimberly Kallianos, Curtis P Langlotz, Matthew P Lungren, Andrew Y Ng, and Bhavik N Patel. Automated coronary calcium scoring using deep learning with multicenter external validation. *NPJ Digit. Med.*, 4(1):88, June 2021.

DINO-LG: A Task-Specific DINO Model For Coronary Calcium Scoring

- [9] Marly van Assen, Simon S Martin, Akos Varga-Szemes, Saikiran Rapaka, Serkan Cimen, Puneet Sharma, Pooyan Sahbaee, Carlo N De Cecco, Rozemarijn Vliegenthart, Tyler J Leonard, Jeremy R Burt, and U Joseph Schoepf. Automatic coronary calcium scoring in chest CT using a deep neural network in direct comparison with non-contrast cardiac CT: A validation study. *Eur. J. Radiol.*, 134(109428):109428, January 2021.
- [10] Daigo Takahashi, Shinichiro Fujimoto, Yui O Nozaki, Ayako Kudo, Yuko O Kawaguchi, Kazuhisa Takamura, Makoto Hiki, Eisuke Sato, Nobuo Tomizawa, Hiroyuki Daida, and Tohru Minamino. Fully automated coronary artery calcium quantification on electrocardiogram-gated non-contrast cardiac computed tomography using deep-learning with novel heart-labelling method. *Eur. Heart J. Open*, 3(6):oead113, November 2023.
- [11] Jelmer M Wolterink, Tim Leiner, Bob D de Vos, Robbert W van Hamersvelt, Max A Viergever, and Ivana Išgum. Automatic coronary artery calcium scoring in cardiac CT angiography using paired convolutional neural networks. *Med. Image Anal.*, 34:123–136, December 2016.
- [12] Richard A P Takx, Ivana Išgum, Martin J Willeminck, Yolanda van der Graaf, Harry J de Koning, Rozemarijn Vliegenthart, Matthijs Oudkerk, Tim Leiner, and Pim A de Jong. Quantification of coronary artery calcium in nongated CT to predict cardiovascular events in male lung cancer screening participants: results of the NELSON study. *J. Cardiovasc. Comput. Tomogr.*, 9(1):50–57, January 2015.
- [13] Caroline Chiles, Fenghai Duan, Gregory W Gladish, James G Ravenel, Scott G Baginski, Bradley S Snyder, Sarah DeMello, Stephanie S Desjardins, Reginald F Munden, and NLST Study Team. Association of coronary artery calcification and mortality in the national lung screening trial: A comparison of three scoring methods. *Radiology*, 276(1):82–90, July 2015.
- [14] Viraj Raygor, Natalie Hoeting, Colby Ayers, Parag Joshi, Arzu Canan, Suhny Abbata, Joanna N Assadourian, Amit Khera, Eric D Peterson, and Ann Marie Navar. Accuracy of incidental visual coronary artery calcium assessment compared with dedicated coronary artery calcium scoring. *J. Cardiovasc. Comput. Tomogr.*, 17(6):453–458, November 2023.
- [15] Ying Liu, Xuezhi Chen, Xianchen Liu, Hao Yu, Lianjun Zhou, Xiaoling Gao, Qinglin Li, Shujun Su, Lin Wang, and Jia Zhai. Accuracy of non-gated low-dose non-contrast chest CT with tin filtration for coronary artery calcium scoring. *Eur. J. Radiol. Open*, 9(100396):100396, January 2022.
- [16] Roman Zeleznik, Borek Foldyna, Parastou Eslami, Jakob Weiss, Ivanov Alexander, Jana Taron, Chintan Parmar, Raza M Alvi, Dahlia Banerji, Mio Uno, Yasuka Kikuchi, Julia Karady, Lili Zhang, Jan-Erik Scholtz, Thomas Mayrhofer, Asya Lyass, Taylor F Mahoney, Joseph M Massaro, Ramachandran S Vasan, Pamela S Douglas, Udo Hoffmann, Michael T Lu, and Hugo J W L Aerts. Deep convolutional neural networks to predict cardiovascular risk from computed tomography. *Nat. Commun.*, 12(1):715, January 2021.
- [17] Connor C Kerndt, Rajus Chopra, Paul Weber, Amy Rechenberg, Daniel Summers, Thomas Boyden, and David Langholz. Using artificial intelligence to semi-quantitate coronary calcium as an ‘incidentaloma’ on non-gated, non-contrast CT scans, a single-center descriptive study in west michigan. *Spartan Med. Res. J.*, 8(1), December 2023.
- [18] Maximilian Nielsen, Laura Wenderoth, Thilo Sentker, and René Werner. Self-supervision for medical image classification: State-of-the-art performance with 100 labeled training samples per class. *Bioengineering (Basel)*, 10(8), July 2023.
- [19] Xiaofan Li, Bo Peng, Jie Hu, Changyou Ma, Daipeng Yang, and Zhuyang Xie. USL-Net: Uncertainty self-learning network for unsupervised skin lesion segmentation. *Biomed. Signal Process. Control*, 89(105769):105769, March 2024.
- [20] Shih-Cheng Huang, Anuj Pareek, Malte Jensen, Matthew P Lungren, Serena Yeung, and Akshay S Chaudhari. Self-supervised learning for medical image classification: a systematic review and implementation guidelines. *NPJ Digit. Med.*, 6(1):74, April 2023.
- [21] Hanguang Xiao, Li Li, Qiyuan Liu, Xiuhong Zhu, and Qihang Zhang. Transformers in medical image segmentation: A review. *Biomed. Signal Process. Control*, 84(104791):104791, July 2023.
- [22] Mathilde Caron, Hugo Touvron, Ishan Misra, Herve Jegou, Julien Mairal, Piotr Bojanowski, and Armand Joulin. Emerging properties in self-supervised vision transformers. In *2021 IEEE/CVF International Conference on Computer Vision (ICCV)*. IEEE, October 2021.
- [23] Afolasayo A Aromiwura and Dinesh K Kalra. Artificial intelligence in coronary artery calcium scoring. *J. Clin. Med.*, 13(12):3453, June 2024.
- [24] Antonio G Gennari, Alexia Rossi, Carlo N De Cecco, Marly van Assen, Thomas Sartoretti, Andreas A Giannopoulos, Moritz Schwyzler, Martin W Huellner, and Michael Messerli. Artificial intelligence in coronary artery calcium score: rationale, different approaches, and outcomes. *Int. J. Cardiovasc. Imaging*, 40(5):951–966, May 2024.
- [25] Roos A Groen, J Wouter Jukema, Paul R M van Dijkman, Jeroen J Bax, Hildo J Lamb, M Louisa Antoni, and Michiel A de Graaf. The clear value of coronary artery calcification evaluation on non-gated chest computed tomography for cardiac risk stratification. *Cardiol. Ther.*, 13(1):69–87, March 2024.
- [26] Khaled Abdelrahman, Arthur Shiyovich, Daniel M Huck, Adam N Berman, Brittany Weber, Sumit Gupta, Rhanderson Cardoso, and Ron Blankstein. Artificial intelligence in coronary artery calcium scoring detection and quantification. *Diagnostics (Basel)*, 14(2), January 2024.
- [27] Shyon Parsa, Adam Saleh, Viraj Raygor, Natalie Hoeting, Anjali Rao, Ann Marie Navar, Anand Rohatgi, Fernando Kay, Suhny Abbata, Amit Khera, and Parag H Joshi. Measurement and application of incidentally detected coronary calcium: JACC review topic of the week. *J. Am. Coll. Cardiol.*, 83(16):1557–1567, April 2024.

DINO-LG: A Task-Specific DINO Model For Coronary Calcium Scoring

- [28] Connor C Kerndt, Rajus Chopra, Paul Weber, Amy Rechenberg, Daniel Summers, Thomas Boyden, and David Langholz. Using artificial intelligence to semi-quantitate coronary calcium as an ‘incidentaloma’ on non-gated, non-contrast CT scans, a single-center descriptive study in west michigan. *Spartan Med. Res. J.*, 8(1), December 2023.
- [29] Joo Hyeok Choi, Min Jae Cha, Iksung Cho, William D Kim, Yera Ha, Hyewon Choi, Sun Hwa Lee, Seng Chan You, and Jee Suk Chang. Validation of deep learning-based fully automated coronary artery calcium scoring using non-ECG-gated chest CT in patients with cancer. *Front. Oncol.*, 12:989250, September 2022.
- [30] Thomas Sartoretti, Antonio G Gennari, Elisabeth Sartoretti, Stephan Skawran, Alexander Maurer, Ronny R Buechel, and Michael Messerli. Fully automated deep learning powered calcium scoring in patients undergoing myocardial perfusion imaging. *J. Nucl. Cardiol.*, 30(1):313–320, February 2023.
- [31] David Eng, Christopher Chute, Nishith Khandwala, Pranav Rajpurkar, Jin Long, Sam Shleifer, Mohamed H Khalaf, Alexander T Sandhu, Fatima Rodriguez, David J Maron, Saeed Seyyedi, Daniele Marin, Ilana Golub, Matthew Budoff, Felipe Kitamura, Marcelo Straus Takahashi, Ross W Filice, Rajesh Shah, John Mongan, Kimberly Kallianos, Curtis P Langlotz, Matthew P Lungren, Andrew Y Ng, and Bhavik N Patel. Automated coronary calcium scoring using deep learning with multicenter external validation. *NPJ Digit. Med.*, 4(1):88, June 2021.
- [32] Sanne G M van Velzen, Nikolas Lessmann, Birgitta K Velthuis, Ingrid E M Bank, Desiree H J G van den Bongard, Tim Leiner, Pim A de Jong, Wouter B Veldhuis, Adolfo Correa, James G Terry, John Jeffrey Carr, Max A Viergever, Helena M Verkooijen, and Ivana Išgum. Deep learning for automatic calcium scoring in CT: Validation using multiple cardiac CT and chest CT protocols. *Radiology*, 295(1):66–79, April 2020.
- [33] Roman Zeleznik, Borek Foldyna, Parastou Eslami, Jakob Weiss, Ivanov Alexander, Jana Taron, Chintan Parmar, Raza M Alvi, Dahlia Banerji, Mio Uno, Yasuka Kikuchi, Julia Karady, Lili Zhang, Jan-Erik Scholtz, Thomas Mayrhofer, Asya Lyass, Taylor F Mahoney, Joseph M Massaro, Ramachandran S Vasan, Pamela S Douglas, Udo Hoffmann, Michael T Lu, and Hugo J W L Aerts. Deep convolutional neural networks to predict cardiovascular risk from computed tomography. *Nat. Commun.*, 12(1):715, January 2021.
- [34] Allison W Peng, Ramzi Dudum, Sneha S Jain, David J Maron, Bhavik N Patel, Nishith Khandwala, David Eng, Akshay S Chaudhari, Alexander T Sandhu, and Fatima Rodriguez. Association of coronary artery calcium detected by routine ungated CT imaging with cardiovascular outcomes. *J. Am. Coll. Cardiol.*, 82(12):1192–1202, September 2023.
- [35] Bernhard Föllmer, Federico Biavati, Christian Wald, Sebastian Stober, Jackie Ma, Marc Dewey, and Wojciech Samek. Active multitask learning with uncertainty-weighted loss for coronary calcium scoring. *Med. Phys.*, 49(11):7262–7277, November 2022.
- [36] Germán González, George R Washko, Raúl San José Estépar, Miguel Cazorla, and Carlos Cano Espinosa. Automated agatston score computation in non-ECG gated CT scans using deep learning. In Elsa D Angelini and Bennett A Landman, editors, *Medical Imaging 2018: Image Processing*. SPIE, March 2018.
- [37] Abdul Rahman Ithdayhid, Nick S R Lan, Michelle Williams, David Newby, Julien Flack, Simon Kwok, Jack Joyner, Sahil Gera, Lawrence Dembo, Brendan Adler, Brian Ko, Benjamin J W Chow, and Girish Dwivedi. Evaluation of an artificial intelligence coronary artery calcium scoring model from computed tomography. *Eur. Radiol.*, 33(1):321–329, January 2023.
- [38] Jiajian Li, Anwei Li, Jiansheng Fang, Yonghe Hou, Chao Song, Huifang Yang, Jingwen Wang, Hongbo Liu, and Jiang Liu. Combating coronary calcium scoring bias for non-gated CT by semantic learning on gated CT. In *2023 IEEE/CVF International Conference on Computer Vision Workshops (ICCVW)*, pages 2575–2583. IEEE, October 2023.
- [39] Rui Santos, Rúben Baeza, Vitor Manuel Filipe, Francesco Renna, Hugo Paredes, and João Pedrosa. Lightweight 3D CNN for the segmentation of coronary calcifications and calcium scoring. In *2024 IEEE 22nd Mediterranean Electrotechnical Conference (MELECON)*. IEEE, June 2024.
- [40] Olaf Ronneberger, Philipp Fischer, and Thomas Brox. U-Net: Convolutional networks for biomedical image segmentation. In *Lecture Notes in Computer Science*, Lecture notes in computer science, pages 234–241. Springer International Publishing, Cham, 2015.
- [41] Nicolas Gogin, Mario Viti, Luc Nicodème, Mickaël Ohana, Hugues Talbot, Umit Gencer, Magloire Mekukosokeng, Thomas Caramella, Yann Diascorn, Jean-Yves Airaud, Marc-Samir Guillot, Zoubir Bensalah, Caroline Dam Hieu, Bassam Abdallah, Imad Bousaid, Nathalie Lassau, and Elie Mousseaux. Automatic coronary artery calcium scoring from unenhanced-ECG-gated CT using deep learning. *Diagn. Interv. Imaging*, 102(11):683–690, November 2021.
- [42] Mariusz Bujny, Katarzyna Jesionek, Jakub Nalepa, Karol Misalski-Jamka, Katarzyna Widawka-Żak, Sabina Wolny, and Marcin Kostur. Coronary artery segmentation in non-contrast calcium scoring ct images using deep learning, 2024. URL <https://arxiv.org/abs/2403.02544>.
- [43] Salman Mohammadi, Shadia Mikhael, Keith Goatman, Sonia Dahdouh, Olivier Jaubert, Jeremy Voisey, Rebecca Hughes, Conor Bradley, and Richard Good. Deep learning-based detection of coronary artery calcification in non-contrast and contrast-enhanced ct scans. *Research Square Platform LLC*, April 2024. doi:10.21203/rs.3.rs-4281908/v1. URL <http://dx.doi.org/10.21203/rs.3.rs-4281908/v1>.
- [44] Daigo Takahashi, Shinichiro Fujimoto, Yui O Nozaki, Ayako Kudo, Yuko O Kawaguchi, Kazuhisa Takamura, Makoto Hiki, Eisuke Sato, Nobuo Tomizawa, Hiroyuki Daida, and Tohru Minamino. Fully automated coronary artery calcium quantification on electrocardiogram-gated non-contrast cardiac computed tomography using deep-learning with novel

DINO-LG: A Task-Specific DINO Model For Coronary Calcium Scoring

- heart-labelling method. *Eur. Heart J. Open*, 3(6):oead113, November 2023.
- [45] Nan Zhang, Guang Yang, Weiwei Zhang, Wenjing Wang, Zhen Zhou, Heye Zhang, Lei Xu, and Yundai Chen. Fully automatic framework for comprehensive coronary artery calcium scores analysis on non-contrast cardiac-gated CT scan: Total and vessel-specific quantifications. *Eur. J. Radiol.*, 134(109420):109420, January 2021.
 - [46] Jia-Sheng Hong, Yun-Hsuan Tzeng, Wei-Hsian Yin, Kuan-Ting Wu, Huan-Yu Hsu, Chia-Feng Lu, Ho-Ren Liu, and Yu-Te Wu. Automated coronary artery calcium scoring using nested U-Net and focal loss. *Comput. Struct. Biotechnol. J.*, 20: 1681–1690, March 2022.
 - [47] Sanskriti Singh. Automated coronary calcium scoring using u-net models through semi-supervised learning on non-gated CT scans. In *2022 IEEE MIT Undergraduate Research Technology Conference (URTC)*. IEEE, September 2022.
 - [48] Shih-Cheng Huang, Anuj Pareek, Malte Jensen, Matthew P Lungren, Serena Yeung, and Akshay S Chaudhari. Self-supervised learning for medical image classification: a systematic review and implementation guidelines. *NPJ Digit. Med.*, 6(1):74, April 2023.
 - [49] Maxime Oquab, Timothée Darcet, Théo Moutakanni, Huy Vo, Marc Szafraniec, Vasil Khalidov, Pierre Fernandez, Daniel Haziza, Francisco Massa, Alaaeldin El-Nouby, Mahmoud Assran, Nicolas Ballas, Wojciech Galuba, Russell Howes, Po-Yao Huang, Shang-Wen Li, Ishan Misra, Michael Rabbat, Vasu Sharma, Gabriel Synnaeve, Hu Xu, Hervé Jegou, Julien Mairal, Patrick Labatut, Armand Joulin, and Piotr Bojanowski. DINOv2: Learning robust visual features without supervision. *Transactions on Machine Learning Research*, 2023.
 - [50] Mohammadreza Shakouri, Fatemeh Iranmanesh, and Mahdi Eftekhari. DINO-CXR: A self supervised method based on vision transformer for chest x-ray classification. In *Lecture Notes in Computer Science*, Lecture notes in computer science, pages 320–331. Springer Nature Switzerland, Cham, 2023.
 - [51] Christos Matsoukas, Johan Fredin Haslum, Magnus Söderberg, and Kevin Smith. Pretrained vits yield versatile representations for medical images, 2023. URL <https://arxiv.org/abs/2303.07034>.
 - [52] Fernando Pérez-García, Harshita Sharma, Sam Bond-Taylor, Kenza Bouzid, Valentina Salvatelli, Maximilian Ilse, Shruthi Bannur, Daniel C Castro, Anton Schwaighofer, Matthew P Lungren, Maria Wetscherek, Noel Codella, Stephanie L Hyland, Javier Alvarez-Valle, and Ozan Oktay. RAD-DINO: Exploring scalable medical image encoders beyond text supervision. 2024. doi:<https://doi.org/10.48550/arXiv.2401.10815>. URL <https://arxiv.org/abs/2401.10815>.
 - [53] Mohammed Baharoon, Waseem Qureshi, Jiahong Ouyang, Yanwu Xu, Abdulrhman Aljouie, and Wei Peng. Evaluating general purpose vision foundation models for medical image analysis: An experimental study of dinov2 on radiology benchmarks, 2023. URL <https://arxiv.org/abs/2312.02366>.
 - [54] Yuning Huang, Jingchen Zou, Lanxi Meng, Xin Yue, Qing Zhao, Jianqiang Li, Changwei Song, Gabriel Jimenez, Shaowu Li, and Guanghui Fu. Comparative analysis of ImageNet pre-trained deep learning models and DINOv2 in medical imaging classification. In *2024 IEEE 48th Annual Computers, Software, and Applications Conference (COMPSAC)*, volume 33, pages 297–305. IEEE, July 2024.
 - [55] Alhassan Mumuni and Fuseini Mumuni. Data augmentation: A comprehensive survey of modern approaches. *Array*, 16: 100258, December 2022. ISSN 2590-0056. doi:10.1016/j.array.2022.100258. URL <http://dx.doi.org/10.1016/j.array.2022.100258>.
 - [56] Manuel Cossio. Augmenting medical imaging: A comprehensive catalogue of 65 techniques for enhanced data analysis, 2023. URL <https://arxiv.org/abs/2303.01178>.
 - [57] Evgin Goceri. Medical image data augmentation: techniques, comparisons and interpretations. *Artificial Intelligence Review*, 56(11):12561–12605, March 2023. ISSN 1573-7462. doi:10.1007/s10462-023-10453-z. URL <http://dx.doi.org/10.1007/s10462-023-10453-z>.
 - [58] Connor Shorten and Taghi M. Khoshgoftaar. A survey on image data augmentation for deep learning. *Journal of Big Data*, 6(1), July 2019. ISSN 2196-1115. doi:10.1186/s40537-019-0197-0. URL <http://dx.doi.org/10.1186/s40537-019-0197-0>.
 - [59] Madeline Chantry Schiappa, Shehreen Azad, Sachidanand VS, Yunhao Ge, Ondrej Miksik, Yogesh S. Rawat, and Vibhav Vineet. Robustness analysis on foundational segmentation models, 2023. URL <https://arxiv.org/abs/2306.09278>.
 - [60] Stanford AIMI. COCA- Coronary Calcium and chest CT’s Dataset. Accessed June 10, 2024. <https://stanfordaimi.azurewebsites.net/datasets/e8ca74dc-8dd4-4340-815a-60b41f6cb2aa>, 2021.